Physica C 205 (1993) 271–279
North-Holland

PHYSICA C

Texture formation in $Bi_2Sr_2Ca_1Cu_2O_x$/Ag tapes prepared by partial melt process

T.D. Aksenova, P.V. Bratukhin, S.V. Shavkin and V.L. Melnikov
Moscow Engineering-Physics Institute, 115409, Moscow, Russian Federation

E.V. Antipova, N.E. Khlebova and A.K. Shikov
A.A. Bochvar Nonorganic Materials Institute, 123060, Moscow, Russian Federation

Received 16 September 1992

Textured $Bi_2Sr_2Ca_1Cu_2O_x$/Ag tapes prepared by "powder-in-tube" method and partial melt process were studied. A new model of texture formation during partial melt technology was proposed for Bi(2212)–Ag composites. The model is based on anisotropic Bi(2212) crystalline growth from melt in quasi-two-dimensional volume and explains a wide set of experimental data. The computer simulation of the growth process according to the suggested model was carried out. The factors promoting the texture increase were revealed.

1. Introduction

The interest in Bi(2212)-based tapes is caused by the possibility of using them in superconducting magnets for high magnetic fields at liquid helium temperatures because the current carrying capacity of this material at high magnetic fields exceeds the capabilities of the traditional low-T_c conductors. For example, critical current densities greater then 10^4 A/cm^2 at 4.2 K in magnetic fields greater then 20 T have been reported for 2212-based tapes [1]. It is known that HTSC has a strong anisotropy of superconducting properties, which is why a strong crystallographic texture of real conductors needs to be formed. The mechanisms of texture formation in HTSC can be various: from stacking texture arising from a powder compaction process to deformation texture during thermal–mechanical treatment [2–5].

The best 2212-based conductors with high J_c have been produced by a so-called partial-melt heat treatment [6]. The microstructure of the oxide zone formed under partial-melt heat treatment has been investigated rather thoroughly. It was observed [7–9] that when the oxide thickness is less than $h_{crit} = 20$ μm, a well-aligned microstructure with plate-like grains is formed. When the oxide layer is thicker than h_{crit}, two zones with different microstructure are observed: a highly textured microstructure near the oxide/Ag interface, and a weakly textured region in the middle of the tape. It was revealed that some factors resulted in texture strengthening. They are the external form of the superconductive composite, the tape thickness, the annealing temperature, the cooling rate, and Ag as a sheath material [6]. But the reasons for the process under partial-melt heat treatment were not discussed. We suggest a concept of the texture formation mechanism during thermal treatment with partial melting of Bi(2221)–Ag composites in this paper.

2. Procedures

Composites were obtained by the "powder-in-tube" method with powder composition $Bi_4Sr_3Ca_3Cu_4O_x$ as a precursor. The process was described in detail early in paper [10]. The samples in the form of Ag-sheathed tapes (0.1×3.4 mm^2 and 0.2×3.4 mm^2 in cross-section) with a Bi(2212) core were annealed at various temperatures, T_a, after final deformation. The cross-section of the oxide core has a lens-like shape with maximum thickness of

about 30 and 50 μm for composites with thicknesses $h=0.1$ mm and $h=0.2$ mm, respectively.

X-ray diffraction analysis was carried out on a powder DRON-3 diffractometer with a texture attachment. X-ray spectra were treated according to procedures described in ref. [11]. Parameters of the X-ray physical diffraction lines (diffraction lines after correction of instrumental aberrations) were obtained. The profile fitting methods [12] were used to deconvolute diffraction multiplets. The convolution of the instrumental function (the function reflecting the instrumental aberration of physical spectra) with Lorentz-like curves, i.e. $[1+((\nu-\nu_0)/b)^2]^{-n}$, $n=1-\infty$ was used for the shape functions. The best fit was obtained for $n=1-2$. Background (polynom of 2–4 degree) was refined simultaneously. The instrumental function was computer simulated [11].

The X-ray data obtained were used for quantitative texture analysis [13]. We calculated such texture parameters as half-width of the texture maximum, β, and volume fraction of crystallites whose [001] normals are distributed in a cone angle $\pm 5°$ around the normal to the tape plane, V_5. Direct pole figures (DPF) were built according to the conventional tilting method [14].

The critical current measurements were carried out by 4-probe mode at 4.2 K in $H=0$ T with a 0.1 μV/cm criterion. Then the critical current densities were calculated. The electrophysical and texture data and also fabrication condition data are shown in table 1.

3. Experimental results

The X-ray phase analysis has shown that the 2212 phase is predominant, the main impurity being 2201 phase with a volume fraction of 10–15%. The following parameters were varied during the sample fabrication: composite thickness, h (0.1 and 0.2 mm), temperature of final annealing, T_a (860, 870, 880°C). After annealing for 10 h the specimens were cooled at a rate of 60°C/h.

There is an explicit correlation between J_c and T_a (fig. 1). The increasing of the annealing temperature from 860°C to 880°C leads to J_c increasing by 8–10 times in magnitude. J_c of the samples with $h=0.1$ mm exhibit an especially sharp dependence.

The direct pole figures (001) and {1115} (fig. 2) were registered in detail for the samples A21 and A1 (table 1) whose critical currents had been quite different. The typical basal (001) texture for such samples had been formed. There is a single strong compact central maximum with a weak diffuse part on DPF (001), the shape of this compact texture peak being almost round. The texture maximum in the A21 sample is significantly stronger and narrower than in the A1 sample. The DPF {1115} shows the distribution of the crystallographic normals in the rolling plane. There is a weak component of the rolling texture in the sample A21. Consequently, the texture type of the studied samples is the same but its power is varied considerably.

To compare quantitatively the sample texture, we registered two rocking curves (cross-sections of (001) DPF) for each sample. Rocking curves along and across the rolling direction differed insignificantly. The half-widths of the maxima in DPF cross-sections, β, and the second texture parameter, V_5, were determined. Figure 3 shows the critical current density J_c versus the texture parameters. The texture becomes stronger (i.e. increasing V_5 and decreasing β) as the J_c becomes greater. It is obvious that J_c dependence is not saturated yet. So it is ascertained that the current carrying capacity of the composites directly depends upon texture, and further texture increase will undoubtedly increase the critical current density. The formation of the stronger texture takes place at higher annealing temperatures (880°C) in the thinner composite tape (0.1 mm). Table 2 contains some structural features of the studied samples: lattice unit parameters, microstrains and coherent scattering domain sizes along the [001] direction.

As one can see from table 2, increasing the annealing temperature gives rise to a slight increase of the lattice unit parameter and substantial increases of the microdistortions and coherent scattering domain sizes.

4. Model of texture formation

The influence of the sample thickness on its texture could be explained by the inhomogeneous structure in the tape cross-section. When the oxide layer

Table 1
Critical properties and texture parameters of the samples

Sample No.	Sample thickess (mm)	Heat treatment, 10 h	4.2 K, 0 T		β (deg)	V_s (%)
			I_c (A)	J_c (10^4 A/cm^2)		
A1	0.1	860°C	2.7	0.5	23	10
A2	0.1	870°C	30.0	5.0	10	34
A21	0.1	870°C	36.5	6.1	7	52
A21a [a)]	0.1	870°C	–	–	10	32
A3a	0.1	880°C	48.1	6.7	11	39
B1	0.2	860°C	5.0	0.6	26	11
B2	0.2	870°C	20.0	2.3	13	22
B3	0.2	880°C	57.8	5.3	8	36
B3a	0.2	880°C	–	–	9	–

[a)] a – Bi (2212) oxide stuck on an Ag sheath.

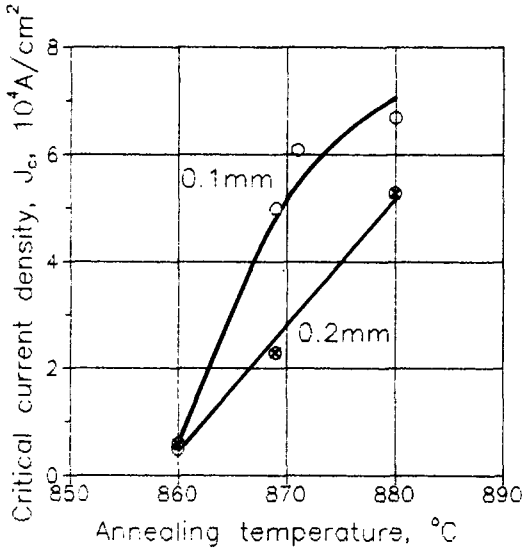

Fig. 1. The critical current density dependence on annealing temperature for the tapes with 0.1 and 0.2 mm thickness.

is thicker than $h_{crit} = 20$ μm, two zones with different microstructures are observed [7–9]. The total thickness of the oxide core in the studied tapes did not exceed $2h_{crit}$, so it can be supposed that a significant part of the HTSC volume has a highly aligned structure. In reality, the bulk texture was observed in the studied samples – variation of texture versus depth was not detected.

A homogeneous texture state was also witnessed by the transport properties: if the high current capacity zone exists just near the Ag–HTSC interface then one should observe the same critical currents I_c, but different critical current densities J_c, for composites with the same texture parameters but different thicknesses. But it is obvious (see fig. 3, samples A1 and B1, A2 and B3) that an identical texture state of composites corresponds to equal J_c (but not I_c) which is independent on the sample thickness. Thus, if the layers without highly aligned grains as in refs. [7–9] exist in the middle of the oxide core in our samples, their volume parts are negligible and these layers do not influence the structural and electrophysical properties.

A "melt model" is proposed here to interpret the existing collection of structure and critical current data described in this paper and in many others [7–9, 15–20].

At first let us consider the process of Bi(2212) ceramic melt crystallization in "flattened volume", i.e., in a volume limited by two Ag sheets, in the ideal conditions. It is known that a great anisotropy of growth rate along different crystallographic directions is inherent to HTSC crystals. That is why single crystals of HTSC grown from melt always have a flat form with crystallographic directions [001] along the smallest facet. The growth rates along the [001] and [100] directions differ by at least one to two orders of magnitude. For example, in ref. [21] Bi(2212) single crystals were observed with dimensions $20 \times 5 \times 0.3$ mm^3, while Nd–Ce–Cu–O single crystals grown by spontaneous crystallization had dimensions $50 \times 50 \times 0.1$ mm^3 [22]. The plate shape of the

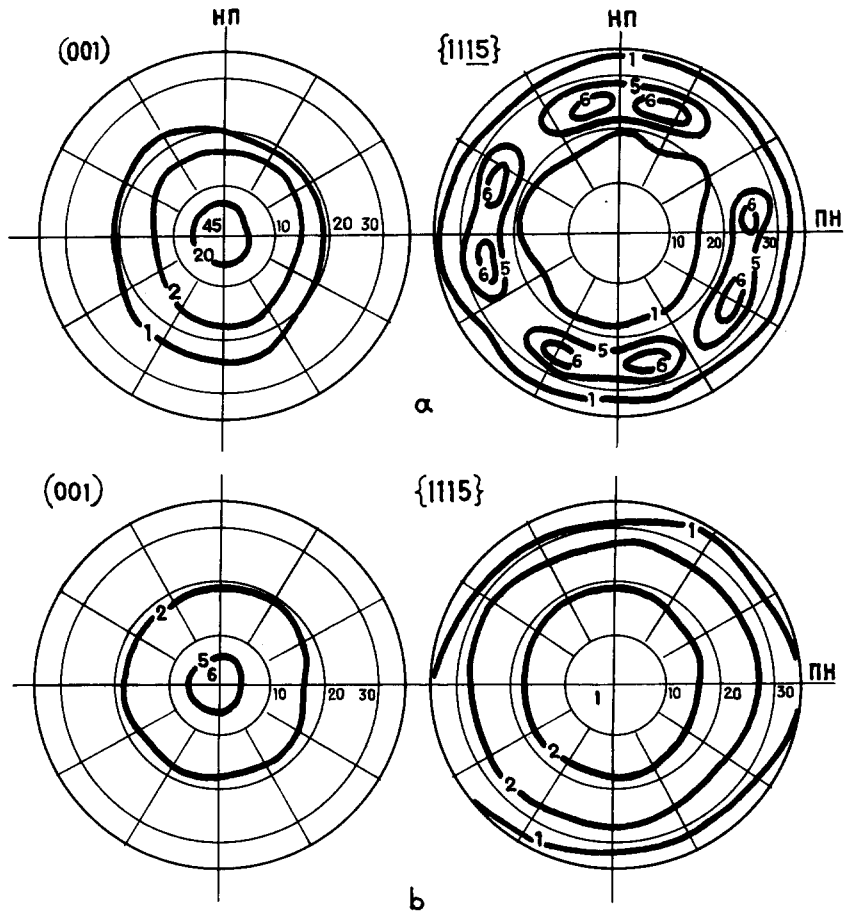

Fig. 2. Direct pole figures (001) and {1115} for samples A21 (a) and A1 (b).

single crystals arises from the anisotropy of growth rate.

We suppose that Bi(2212) grains are almost or quite completely melted during the process. The orientation of nuclei of crystallization appearing in the melt during cooling is supposed to be random (fig. 4). Impurities and the part of the oxide not melting may also serve as crystallization centers. A crystallite whose orientation is not favorable (i.e. with the [001]-axis diverging from the normal to the composite plane) grows rapidly until its growth surface comes into contact with the Ag sheet, when the growth process slows down and continues slowly along the [001] dimension. Crystallites with the [001]-axis direction coinciding with the plate normal grow rapidly along the composite plane and accept almost all volume of melt. As a result, even if centers of crystallization initially have no preferred orientation, a strong concentration of [001]-axes near the plate normal will be observed – the anisotropic growth of crystallites in the quasi-two-dimensional melt volume provides it. Moreover, recrystallization processes may take place. So a strong basic texture forms in composites during thermal treatment.

Our "melt model" is based upon the following suppositions:

(1) high anisotropy of crystalline growth rate;

(2) quasi-two-dimensional crystallization space.

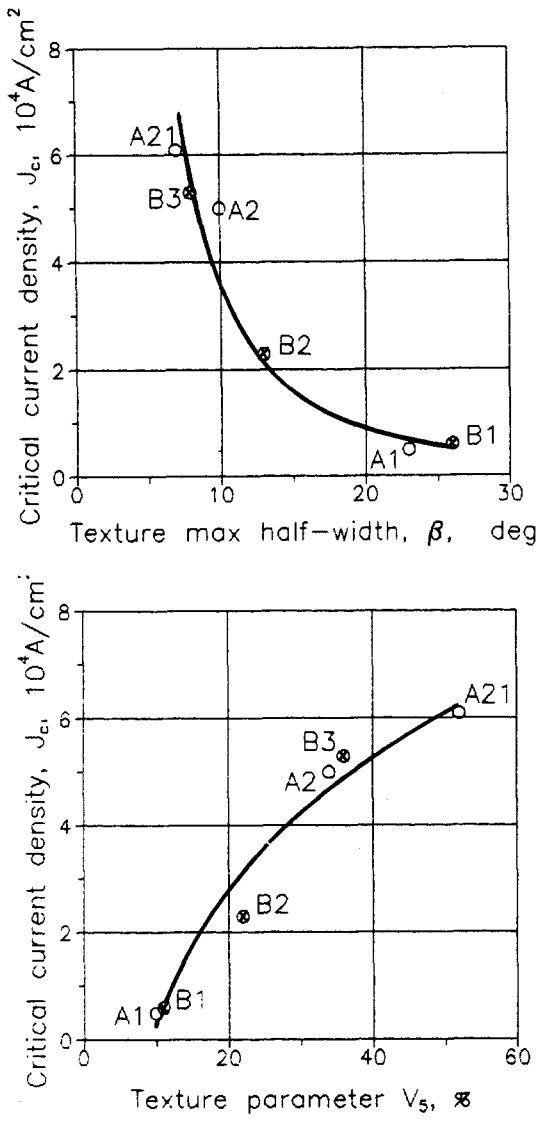

Fig. 3. The dependence of critical current density on texture parameters: half-width of texture maximum, β (a), and volume part of crystallites with [001] normals distributed in a cone angle $\pm 5°$ around the tape plane normal, V_5 (b).

5. A computer simulation of texture growth

A computer simulation was carried out for the model and quantitative estimates to be obtained. A mathematical model of anisotropic grain dynamic crystallization in quasi-two-dimensional crystallization space was invented.

Let us consider crystalline growth in a thin layer (layer thickness, d, is much smaller than its other dimensions). We suppose spontaneous crystallization in the whole substance volume, ignoring possible effects connected with temperature gradient during cooling and also the process of the recrystallization, i.e. initial nucleus concentration does not change, the nuclei are disposed homogeneously and they have random orientation. The crystal growth proceeds with constant rate depending on direction $v(\boldsymbol{S})$; moreover, an oxide crystallite has a particular direction ([001]-axis in the Bi(2212) phase), along which the growth rate, $v_{\parallel}$, is much smaller than the growth rate along perpendicular directions (any direction in the (001)-plane), $v_{\perp}$. The growth process can be stopped by the coming into contact of one crystallite with another or with the Ag sheath. The volume part of crystallites with particular orientation in the substance, $v(\theta)$, can be calculated; θ is the deflection angle of the crystalline [001]-axis from the sheath normal. The crystalline growth can be expressed by the following term:

$$\frac{dV(\theta)}{dt} = \oint d\boldsymbol{S}(v(\boldsymbol{S})P_v P_d) , \tag{1}$$

where $v(\boldsymbol{S})$ is the crystalline growth rate in the $\boldsymbol{S}$ direction, P_v the probability that a single crystallite will not be counteracted by a neighboring crystallite during growth, and P_d the probability that a single crystallite will not be counteracted by a Ag sheath during growth. We shall write:

$$P_v = 1 - \frac{\sum V_{cryst}}{V_{sample}} , \tag{2}$$

because of the absence of correlation between crystalline nuclei.

So P_v is a function of time solely. Then P_v can be excluded from eq. (1) as follows: $P_v(t)dt = d\tau$.

$$\frac{dV(\theta)}{d\tau} = \oint d\boldsymbol{S}(v(\boldsymbol{S})P_d) . \tag{3}$$

Thus we reduce our problem to that of solitary microcrystallite growth limited by layer surfaces. Moreover, we are interested only in the final results when the growth of all the crystallites has stopped (limits $t \to \infty$ or $\tau \to \infty$, then $P_v = 0$) and the crystallites fill all the oxide layer.

Table 2
Structure parameters of studied samples

Sample	Lattice parameters (nm)		Microdistortion $\langle\epsilon\rangle_{\langle 001\rangle}$ (10^{-3})	Coherent scatt. domain size $\langle D\rangle_{\langle 001\rangle}$ (nm)
	a	c		
A1	0.5386(3)	3.0716(9)	1.7(2)	29(4)
B1	0.5397(8)	3.0701(5)	1.7(3)	32(3)
A2	0.5396(2)	3.0718(7)	7.0(2)	65(5)
A21	0.5397(3)	3.0748(5)	3.4(3)	69(4)
B2	0.5391(3)	3.0705(9)	5.7(2)	86(3)
A3	0.5413(9)	3.0788(4)	13.0(4)	76(2)
B3	0.5404(6)	3.0757(5)	4.9(3)	63(2)

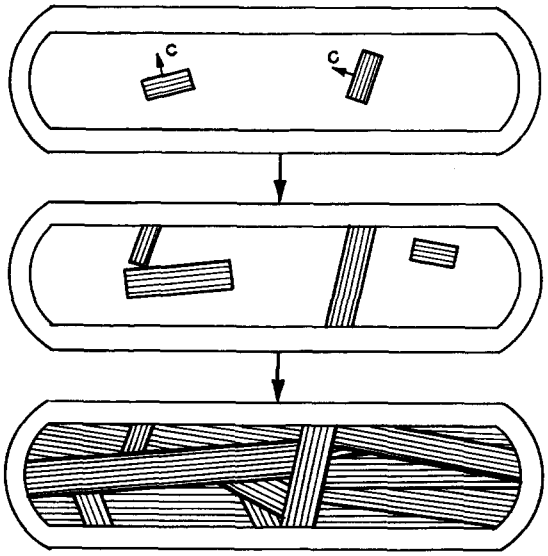

Fig. 4. Schematic view of texture formation during oxide crystallization process.

To solve this problem, we suppose that a flat crystallite is placed along the main crystallographic axis. The following equations can be obtained after averaging along the distance from the layer surfaces (let us denote $l=2v_\perp\tau/d$ and $\varphi=\operatorname{arctg}(v_\parallel/v_\perp)$:

$$V(\theta,L)\frac{1}{\sin\theta}\left[\operatorname{tg}(\min(\theta,\varphi))\right.$$
$$+\frac{1}{6l\cos\theta}\left[f\left(1-l\frac{\sin(\theta+\varphi)}{\cos\varphi}\right)\right.$$
$$\left.\left.-f\left(1-l\frac{\sin|\theta-\varphi|}{\cos\varphi}\right)\right]\right],$$

where function f is determined as

$$f=\begin{cases}x^3, & x>0\\ 0, & x<0\end{cases}, \tag{4}$$

and l is determined from normalization conditions:

$$\rho_0\int_0^{\pi/2}V(\theta,l)\sin\theta\,d\theta=1\,, \tag{5}$$

where ρ_0 is crystalline nucleus concentration.

Figure 5 shows curves calculated according to eqs.

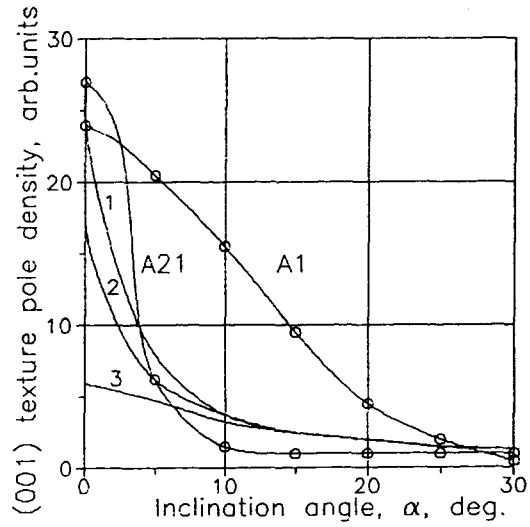

Fig. 5. Theoretical profiles of texture maximum: $v_\parallel/v_\perp=\text{const}=0.02$ and tape thickness correlation $d_1:d_2:d_3=1:2:4$ (curves 1, 2, 3 accordingly); and experimental profiles of texture maximum for the samples A1 and A21.

(4) and (5) for $v_\perp/v_\parallel = 1$–50 in comparison with our experimental DPF cross-sections. The theoretical curves visibly demonstrate the texture strengthening with decreasing oxide layer thickness. It can be noted that the half-width of the theoretical curves is 6–20 degrees, which is in quantitative agreement with the experimental data (see fig. 5 and table 1).

According to the model, anisotropy of crystalline growth rate is essential for texture formation – substances with isotropic rates will not form texture at any layer thickness (see fig. 5). The theoretical half-width of the texture maximum dependences versus oxide layer thickness and growth rate anisotropy (fig. 6) demonstrate texture increase with $v_\parallel/v_\perp$ and decrease with layer thickness. It should be noted that in the framework of the presented model there is no texture saturation effect in the whole range of parameters. As follows from the obtained equations (4) and (5), the texture degree also increases with decrease of nucleus density ρ_0 which could be altered by the cooling rate. It is obvious that ρ_0 increases with cooling rate.

Thus, the high texture arises due to the crystallization process from the melting state inside a quasi-two-dimensional volume even without any temperature gradients.

6. Discussion

Let us use this model for the interpretation of the experimental data. Ag sheets play the role of the case and provide the flat shape of the melt volume that gives rise to an extended texture because of growth features of a 2212 crystallite (growth mainly in the (001) crystallographic plane). According to our model, change of melt space geometry must lead to texture disappearance. This conclusion is verified in ref. [1] – the 2212 phase present in round wires after a partial melt heat treatment did not exhibit any significant texture.

It is also obvious that there is a second conclusion in the framework of our model: increasing the thickness of a flat shape composite must decrease the degree of texture. There are several publications [15–17] where critical current density grows with decreasing tape thickness. When the thickness of the composite decreases to ~0.2 mm, the J_c–h curve has

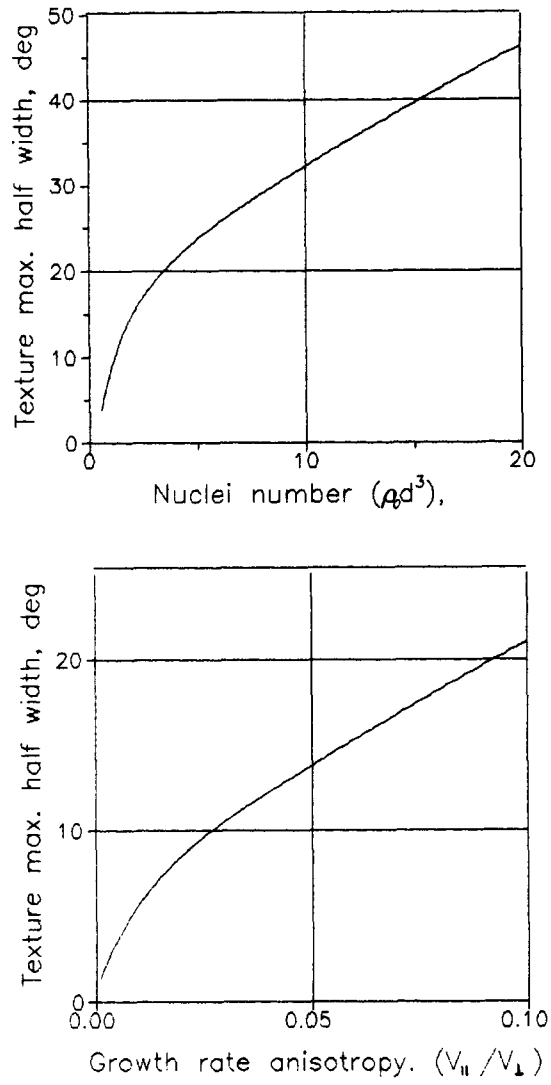

Fig. 6. Theoretical half-width of the texture maximum as a function of parameter $\rho_0 d^3$, characterized oxide layer thickness ($v_\parallel/v_\perp = 0.02$) (a), and growth rate anisotropy ($\rho_0 d^3 = 0.6$) (b).

a slight inclination, further decrease of thickness leading to sharp J_c growth. The sloping part of the J_c–h curve is connected with the changing of non-textured regions in the oxide layer [7]. Our model may explain the sharp fragment of the J_c–h curve. Really, the thinner the composite, the more quickly unfavorably oriented crystallites come into contact with the Ag sheet and slow down the growth and then the higher the texture degree and consequently the

higher the critical current density will be. These phenomena are observed in refs. [15–17] and fig. 1.

Texture intensification in the studied samples with rise of annealing temperature is connected with increasing melt volume fraction. At low temperature (860°C) the melting of grain boundaries takes place. Tight surface forces may cause the reorientation of a plane crystallite according to its form. This is an additional texture producing mechanism. On raising the annealing temperature from 860 to 870–880°C, the volume part of the melt phase grows and consequently, in accordance with the proposed model, texture intensity grows too. It is probable that centers of crystallization that have been created during the preliminary thermo-mechanical treatment can have a preferred orientation. This can further improve the texture perfection.

According to the model, samples with higher texture must consist of larger crystallites. From table 2 one can see that samples treated at 870°C contain crystallites ~2–3 times thicker than samples treated at 860°C.

It is necessary to note that many articles [7,18] inform us that Ag causes the decreasing of the Bi(2212) melting point. So, it can be supposed that Bi(2212) oxide lying near a Ag–oxide interface may be in a fully melted state at the annealing temperatures. At the same time the composite core may be in a solid state. According to the proposed model, the solidification of Bi(2212) melt in a thin layer near the Ag–oxide interface will provide the high degree of texture in this layer, but the composite core will not be highly textured. The changing of texture perfection from the Ag–oxide interface to the core of thick composite ($h \geqslant 20$ μm) [7–9] can be explained by this feature.

It can be expected from the "melt model" that decreasing the cooling rate (smaller density of nuclei) and cycle heat treatment within the temperature area of Bi(2212) crystallization will result in texture imperfection. The first of these suggestions is confirmed in a lot of papers [19,20], where it was shown that texture degree, and accordingly J_c, are higher in samples with slow cooling rate (2–20°C/h) than with more rapid cooling.

Nevertheless, the oxide layer thickness will have to not exceed 30–50 μm (fig. 6) because of the essential half-width of the texture maximum increasing and, consequently, the critical current density decreasing ($\leqslant 10^4$ A/cm^2), which are inconvenient for technological applications. Therefore, to produce HTSC cable there has been constructed a multifilament composite with flat fiber configuration and with fibers no thicker than 30–50 μm (the thinner the better, because there is no texture saturation effect with the oxide thickness decrease).

7. Conclusions

$Bi_2Sr_2Ca_1Cu_2O_x$ textured tapes were prepared by "powder-in-tube" method and partial melt process. Texture increase results in a current carrying capacity increase. A new model of texture formation during partial melt technology was proposed for Bi(2212)–Ag composites. The model is based on anisotropic Bi(2212) crystalline growth from the melt in quasi-two-dimensional volume and explains a wide set of experimental data. The computer simulation of the growth process according to the suggested model was carried out. Results of the computer simulation are in good agreement with experimental data. It was obtained that the following factors promote the texture increase:

(1) reduction of the crystallization nucleus density by slowing down the cooling rate, decreasing the Bi(2212) layer thickness and decreasing the concentrations of impurity solid particles in the melt;

(2) formation of preferred orientation of the crystallization nuclei by preliminary thermo-mechanical treatment or cycle heat treatment within the temperature area of Bi(2212) crystallization.

Acknowledgements

The authors are grateful to E.Yu. Klimenko, A.D. Nikulin and V.S. Kruglov for helpful discussions and continuous attention to the investigations, and to Yu.S. Sokolov and A.M. Malofeev for help in text amending.

This work was supported by the Russian Scientific Council on High T_c Problems and performed within

the project No. 796 of the Russian State Program "High T_c Superconductivity".

References

[1] J. Tenbrink, M. Wilhelm, K. Heine and H. Krauth, IEEE Trans. Magn. 27 (1991) 1239.
[2] C.L. Seaman, S.T. Weir, E.A. Early, M.B. Maple, W.J. Nellis, P.C. McCandless and W.F. Brocious, Appl. Phys. Lett. 57 (1990) 93.
[3] N. Kawahara, S. Kawabata, H. Enami, T. Shinohara, H. Hoshizaki, M. Hasegawa, S. Asai and T. Imura, Jpn. J. Appl. Phys. 29 (1990) L284.
[4] K. Osamura, S. Soo Oh and S. Ochiai, Supercond. Sci. Technol. 3 (1990) 143.
[5] S. Soo Oh, T. Kubota and K. Osamura, Physica C 171 (1990) 265.
[6] K.H. Sandhage, G.N. Riley Jr and W.L. Carter, JOM, March (1991) 21.
[7] J. Kase, T. Morimoto, K. Togano, H. Kumakura, D.R. Dietderich and H. Maeda, IEEE Trans. Magn. 27 (1991) 1254.
[8] H. Kumakura, K. Togano, D.R. Dietderich, H. Maeda, J. Kase and T. Morimoto, Supercond. Sci. Technol. 4 (1991) S157.
[9] R. Flukiger, T. Graf. M. Decroux, C. Groth and Y. Yamada, IEEE Trans. Magn. 27 (1991) 1258.
[10] A.D. Nikulin, A.K. Shikov, N.E. Khlebova, E.V. Antipova, M.V. Burikov, V.N. Shishov, N.I. Kozlenkova and V.V. Medkov, IEEE Trans. Magn. 28 (1992) 862.
[11] E.V. Antipova, P.V. Bratukhin, V.V. Evstigneev, V.D. Zelesnyakov, I.V. Zakhartchenko, Yu.V. Ilukhin, N.E. Khlebova, S.V. Shavkin and A.K. Shikov, Supercond.: Phys. chem., techn. 2 (1989) 135.
[12] S. Oatley and S. French, Acta Crystallogr. A 38 (1982) 537.
[13] T.D. Aksenova, P.V. Bratukhin, I.V. Zakhartchenko and S.V. Shavkin, Supercond.: Phys. chem., techn. 3 (1990) S 263.
[14] A.A. Rusakov, "Roentgenography of metals" (Atomizdat, 1977) p. 479.
[15] Y. Torn, H. Kugai, H. Takei and K. Tada, Jpn. J. Appl. Phys. 29 (1990) L952.
[16] T. Matsumoto, K. Aihara and M. Seido, Hitachi Review 39 (1990) 55.
[17] M. Kawashima, M. Nagata, Y. Hosoda, S. Takano, N. Shibuta, H. Mukai and T. Hikata, IEEE Trans. Magn. 25 (1989) 2168.
[18] W. GAO, S.C. Li and D.A. Rudman, ibid. 167 (1990) 395.
[19] D.R. Dietderich, B. Ullmann, H.C. Freyhardt, J. Kase, H. Kumakura, K. Togano and H. Maeda, Jpn. J. Appl. Phys. 29 (1990) L1100.
[20] J. Kase, K. Togano, H. Kumakura, D.R. Dietderich, N. Irisawa, T. Morimoto and H. Maeda, Jpn. J. Appl. Phys. 29 (1990) L1096.
[21] L.N. Demyanetc, A.B. Byikov, G.V. Kanunnikov, O.K. Melnikov, A.N. Andronov and A.N. Khodan, Supercond. : phys. chem., techn. 2 (1989) 169.
[22] K.V. Gamaunov, A.L. Ivanov, V.V. Osiko and B.M. Tatarintzev, Supercond.: phys. chem., techn. 4 (1991) 2306.